



**HAL**  
open science

## A high resolution and quasi-zonal transect of dissolved Ba in the Mediterranean Sea

Stephanie Jacquet, Christophe Monnin, V Riou, Loïc Jullion, T Tanhua

► **To cite this version:**

Stephanie Jacquet, Christophe Monnin, V Riou, Loïc Jullion, T Tanhua. A high resolution and quasi-zonal transect of dissolved Ba in the Mediterranean Sea. *Marine Chemistry*, 2016, 178, pp.1-7. 10.1016/j.marchem.2015.12.001 . hal-01254976

**HAL Id: hal-01254976**

**<https://hal.science/hal-01254976>**

Submitted on 14 Jan 2016

**HAL** is a multi-disciplinary open access archive for the deposit and dissemination of scientific research documents, whether they are published or not. The documents may come from teaching and research institutions in France or abroad, or from public or private research centers.

L'archive ouverte pluridisciplinaire **HAL**, est destinée au dépôt et à la diffusion de documents scientifiques de niveau recherche, publiés ou non, émanant des établissements d'enseignement et de recherche français ou étrangers, des laboratoires publics ou privés.

1 **A high resolution and quasi zonal transect of dissolved Ba in the**  
2 **Mediterranean Sea**

3  
4  
5 3

6  
7 4 Jacquet S.H.M.<sup>1</sup>, C. Monnin<sup>2</sup>, V. Riou<sup>1</sup>, L. Jullion<sup>1</sup> and T. Tanhua<sup>3</sup>  
8  
9

10 5

11 6 <sup>1</sup> Aix Marseille Université, CNRS/INSU, Université de Toulon, IRD,  
12 Mediterranean Institute of Oceanography (MIO), UM 110, 13288 Marseille,  
13 France  
14  
15 7  
16  
17 8  
18

19 9

20  
21 10 <sup>2</sup> Géosciences Environnement Toulouse, Université de  
22 Toulouse/CNRS/IRD/OMP, 14, Avenue Edouard Belin, 31400 Toulouse, France  
23  
24 11  
25

26 12

27  
28 13 <sup>3</sup> GEOMAR Helmholtz Centre for Ocean Research Kiel, Marine biogeochemistry,  
29 Kiel, Germany  
30  
31 14  
32

33 15

34  
35  
36 16 Corresponding author: S. Jacquet, [stephanie.jacquet@mio.osupytheas.fr](mailto:stephanie.jacquet@mio.osupytheas.fr)  
37  
38

39 17

40  
41 18 Key words: dissolved barium, barite saturation index, Mediterranean Sea  
42  
43

44 19

45  
46 20

47  
48 21

**Submitted to Marine Chemistry**

1  
2  
3  
4  
5  
6  
7  
8  
9  
10  
11  
12  
13  
14  
15  
16  
17  
18  
19  
20  
21  
22  
23  
24  
25  
26  
27  
28  
29  
30  
31  
32  
33  
34  
35  
36  
37  
38  
39  
40  
41  
42  
43  
44  
45  
46  
47  
48  
49  
50  
51  
52  
53  
54  
55  
56  
57  
58  
59  
60  
61  
62  
63  
64  
65

## 22 Abstract

23       The dissolved barium (D\_Ba) data set for the Mediterranean Sea is here  
24 expanded with data from a large-scale transect sampled in April 2011 (M84/3  
25 cruise) at high resolution. A total of 833 seawater samples have been analyzed for  
26 D\_Ba. Over the basin the D\_Ba content ranges from 38 to 85 nmol kg<sup>-1</sup> with local  
27 deep D\_Ba maxima reaching up to 172 nmol kg<sup>-1</sup>. Deep D\_Ba maxima are  
28 associated with near bottom waters influenced by benthic processes and brine  
29 waters. The water column is largely undersaturated with respect to barite (BaSO<sub>4</sub>,  
30 the main phase of particulate biogenic barium P\_Ba), with water column barite  
31 saturation state ranging between 0.2 and 0.6 over the basin. This new D\_Ba  
32 dataset shows that the general zonal distribution of D\_Ba is impacted by the large-  
33 scale Mediterranean circulation, as evidenced by the Levantine Intermediate  
34 Water zonal and meridional progression as well as by the eastward flow of surface  
35 Atlantic Water. However biogeochemical processes are also at play, as suggested  
36 by an elevated D\_Ba content of deep waters and by local lower D\_Ba contents in  
37 intermediate waters. These features could be attributed to active cycling between  
38 the particulate and dissolved Ba phases. Since P\_Ba barite has been recognized in  
39 previous studies as a proxy for particulate organic carbon remineralization at  
40 intermediate depths, the significance of local changes in the water column D\_Ba  
41 patterns may be key to better constrain the Ba and carbon dynamics in the  
42 Mediterranean Sea.

## 43 1. Introduction

44 In the context of studies of the interactions between climate change and the  
45 oceanic biological carbon (C) pump, the barium (Ba) proxy is a key tracer to  
46 estimate the transfer of particulate matter and C from the water column to the  
47 sediments. Particulate biogenic barium (P\_Ba) in suspended matter is mainly  
48 composed of barite (BaSO<sub>4</sub>) crystals (Dehairs et al., 1980). Barite forms during  
49 particulate organic carbon (POC) degradation by marine prokaryotes at  
50 mesopelagic depths (100-1000 m; the depth range within which most of the POC  
51 transported from the mixed layer is degraded). In an ocean that is globally  
52 undersaturated with respect to barite (Monnin et al., 1999, Rushdi et al., 2000;  
53 Monnin and Cividini, 2006) POC sinking aggregates provide favourable  
54 microenvironments for barite precipitation. As a result, P\_Ba barite is one of the  
55 few geochemical proxies for POC remineralization fluxes at mesopelagic depths  
56 (Dehairs et al., 1997, 2008; Cardinal et al., 2005; Jacquet et al., 2008, 2011,  
57 2015).

58 It has been shown that dissolved Ba (D\_Ba) behaves as a bio-intermediate  
59 element, i.e. showing low concentrations in surface waters without reaching total  
60 depletion and increasing concentrations with depth (Chan et al., 1977, Östlund et  
61 al., 1987; Jeandel et al., 1996; Jacquet et al., 2005). This distribution is mainly  
62 attributed to P\_Ba cycling involving barite formation and dissolution. The Ba  
63 dynamics have been investigated in a previous study in the Southern Ocean by  
64 comparing temporal changes of dissolved and particulate barium contents and by  
65 calculating the degree of Ba conservation (Jacquet et al., 2007). It has been  
66 concluded that D\_Ba displays a non-conservative behaviour at horizons of  
67 mesopelagic POC remineralization, pointing to a measureable removal of D\_Ba

1  
2  
3  
4  
5  
6  
7  
8  
9  
10  
11  
12  
13  
14  
15  
16  
17  
18  
19  
20  
21  
22  
23  
24  
25  
26  
27  
28  
29  
30  
31  
32  
33  
34  
35  
36  
37  
38  
39  
40  
41  
42  
43  
44  
45  
46  
47  
48  
49  
50  
51  
52  
53  
54  
55  
56  
57  
58  
59  
60  
61  
62  
63  
64  
65

68 from the local seawater by barite formation (Jacquet et al., 2007). However, much  
69 remains unknown with regards to the significance of local changes in D\_Ba  
70 patterns to further constrain Ba dynamics and POC transfer efficiency in the water  
71 column.

72 The Mediterranean Sea (MedSea) is a landlocked sea with limited, but  
73 crucial, exchange with the Atlantic Ocean, two deep overturning cells, one  
74 shallow circulation and a complex upper layer circulation with several permanent  
75 and quasi-permanent eddies. During the Holocene period (10.8 to 6.1 cal ka BP),  
76 the eastern Mediterranean suffered a major phase of climatic shift in thermohaline  
77 circulation causing abrupt changes in bottom water oxygenation and deposition of  
78 organic-rich anoxic sediment (sapropel). In the light of these past events, the  
79 biogeochemistry and dynamics of the circulation in the Western and Eastern  
80 Mediterranean (WMed, EMed), their connection and the possible implication for  
81 the regional climate system are thus key issues under debate (Tanhua et al.,  
82 2013b; Malanotte-Rizzoli).

83 The MedSea is also a basin of contrasting ecosystems, from strongly  
84 oligotrophic deep interiors to eutrophic northern Adriatic (Durrieu de Madron et  
85 al., 2011; Reygondeau et al., 2013). The coupling between surface biology and  
86 internal remineralization, timescales of their variability between sub-basins and  
87 discrepancies between mesopelagic trophic regime and respiration dynamics  
88 (Santinelli et al., 2010, 2014; Lopez-Sandoval et al., 2011; Luna et al., 2012) are  
89 for instance issues that need to be resolved for a better understanding of the bio-  
90 geochemical processes involved in the carbon dynamics of the Mediterranean  
91 basin. Open questions relates to the impact of the predicted changes in key  
92 physical (e.g. increased stratification, salinity) on this dynamics.

1  
2  
3  
4  
5  
6  
7  
8  
9  
10  
11  
12  
13  
14  
15  
16  
17  
18  
19  
20  
21  
22  
23  
24  
25  
26  
27  
28  
29  
30  
31  
32  
33  
34  
35  
36  
37  
38  
39  
40  
41  
42  
43  
44  
45  
46  
47  
48  
49  
50  
51  
52  
53  
54  
55  
56  
57  
58  
59  
60  
61  
62  
63  
64  
65

93           The present work provides a unique D\_Ba dataset for the Mediterranean  
94 basin. The high sampling resolution offers unprecedented opportunity to discuss  
95 differences in the water column D\_Ba distribution and the water column  
96 saturation with respect to barite between WMed and EMed, and to investigate the  
97 respective roles of physico-chemical and biogeochemical controls. This work is  
98 part of a broader investigation aiming at improving the use of Ba as a proxy to  
99 estimate local processes of POC remineralization in the Mediterranean Sea.

100

## 101   **2. Experiment and methods**

### 102   **2.1 Study area**

103           The whole water column was sampled for D\_Ba along an east to west  
104 transect across the Mediterranean Sea from off the coast of Lebanon to the Strait  
105 of Gibraltar, enabling creation of a quasi-zonal section (M84/3 cruise, Istanbul to  
106 Vigo, 5-28 April 2011, R/V *Meteor*) (Figure 1) (Tanhua et al., 2013a). However,  
107 the Sicily Channel could not be sampled due to political instability in the region.  
108 Additionally, we present a short meridional section from the Adriatic Sea through  
109 the Strait of Otranto to the Ionian Sea (later referred to as the Ionian section). The  
110 period of the M84/3 cruise, April 2011, coincides with the end of the winter-  
111 spring bloom. The cruise was set up to follow the guide-lines of the GO-SHIP  
112 Program (Global Ocean Ship Based Hydrographic Investigation Program), which  
113 aims at creating a globally coordinated network of sustained hydrographic  
114 sections as part of the global ocean/climate observing system. The principal  
115 scientific objective for M84/3 was to understand and document large-scale  
116 Mediterranean water property distributions, their changes and the drivers of those  
117 changes. In particular, M84/3 focused on major shifts in the overturning

1  
2  
3  
4  
5  
6  
7  
8  
9  
10  
11  
12  
13  
14  
15  
16  
17  
18  
19  
20  
21  
22  
23  
24  
25  
26  
27  
28  
29  
30  
31  
32  
33  
34  
35  
36  
37  
38  
39  
40  
41  
42  
43  
44  
45  
46  
47  
48  
49  
50  
51  
52  
53  
54  
55  
56  
57  
58  
59  
60  
61  
62  
63  
64  
65

118 circulation of the Mediterranean basin which began at the end of the 1980s for the  
119 EMed (Roether et al., 1996) and in the mid-2000s for the WMed (Schroeder et al.,  
120 2008). Our specific objective was to document for the first time the D\_Ba  
121 distribution in the Mediterranean basin at a large scale. D\_Ba data are available in  
122 the CDIAC (Carbon Dioxide Information Analysis center) data repository, next to  
123 other physical and chemical parameters obtained during the M84/3 cruise  
124 ([http://cdiac.ornl.gov/oceans/Coastal/Meteor\\_Med\\_Sea.html](http://cdiac.ornl.gov/oceans/Coastal/Meteor_Med_Sea.html)).

125 Detailed description of the Mediterranean circulation as well as water mass  
126 properties and distribution is given in Tanhua et al. (2013b) and Hainbucher et al.  
127 (2014). Briefly, the following main water masses can be distinguished (see  
128 potential temperature – salinity diagram in Fig.2; note that the mesopelagic layer  
129 is hereafter referred to as the intermediate layer): (1) the western part of the zonal  
130 section is dominated by the inflow of surface Atlantic Water (AW) associated  
131 with an intense meso-scale activity along the African coast, and the outflow of  
132 Mediterranean Overflow Water (MOW). AW is mainly detected by fresher  
133 waters; (2) from west to east, AW is gradually replaced by Ionian Surface Water  
134 (ISW) and Levantine Surface Water (LSW). LSW is formed by intensive heating  
135 and evaporation and has the highest salinity and temperature of the entire  
136 MedSea; (3) Levantine Intermediate Water (LIW) is present at intermediate layers  
137 over the whole basin and represents the intermediate water mass connection  
138 between sub-basins. LIW is characterized by high density and a salinity  
139 maximum. During the M84/3 cruise, the core of LIW was detected around 200 m  
140 depth in the EMed and around 500 m depth in the WMed. Cretan Intermediate  
141 Water (CIW) is also found at intermediate depths in the EMed; (4) in the deep  
142 waters we find Eastern Mediterranean Deep Water (EMDW) and Western

1  
2  
3  
4  
5  
6  
7  
8  
9  
10  
11  
12  
13  
14  
15  
16  
17  
18  
19  
20  
21  
22  
23  
24  
25  
26  
27  
28  
29  
30  
31  
32  
33  
34  
35  
36  
37  
38  
39  
40  
41  
42  
43  
44  
45  
46  
47  
48  
49  
50  
51  
52  
53  
54  
55  
56  
57  
58  
59  
60  
61  
62  
63  
64  
65

143 Mediterranean Deep Water (WMDW), in each sub-basin. EMDW is a mixture of  
144 Adriatic Deep Water (AddW), Cretan Deep Water (CDW) and shallower water  
145 masses. WMDW is mainly formed in the Gulf of Lion by open-ocean convection  
146 (Schott et al., 1996) with intermittent contribution from shelf water cascading  
147 (Durrieu de Madron et al., 2013).

## 149 **2.2 Sampling and analyses**

150 Seawater was sampled with a CTD rosette equipped with 24 12-liter water  
151 bottles. Then, fifteen mL of unfiltered seawater were collected in pre-cleaned  
152 polypropylene bottles (Nalgene; rinsed three times with the same seawater  
153 sample), acidified with 15  $\mu\text{L}$  of HCl (Optima grade) and kept at room  
154 temperature for later analysis. No filtration of the seawater was done based on the  
155 well-documented knowledge that D\_Ba represents, in general, a very large  
156 fraction (>99%) of total Ba. There were 47 vertical D\_Ba profiles with a total of  
157 833 D\_Ba samples.

158 D\_Ba was measured using an isotope dilution (ID) method (Klinkhammer  
159 and Chan, 1990 and Freydier et al., 1995) by high resolution sector field -  
160 inductively coupled plasma- mass spectrometry (SF-ICP-MS). This method was  
161 adapted to a Thermo Finnigan Element XR instrument. The D\_Ba measurements  
162 presented here are the sum of dissolved Ba (D\_Ba) and a very small fraction  
163 (generally <1% of total Ba) that is generated from the particulate Ba pool as a  
164 result of the acidification. For the sake of simplicity, we use the term of D\_Ba.  
165 Samples (0.5 mL) were spiked with 300  $\mu\text{L}$  of a  $^{135}\text{Ba}$ -enriched solution (93%  
166  $^{135}\text{Ba}$ ; 95  $\text{nmol kg}^{-1}$ ), and 300  $\mu\text{L}$  of a Nd solution (natural isotopic composition;  
167 70  $\text{nmol kg}^{-1}$ ) was added as an internal standard to correct for mass bias. Finally,



168 samples were diluted with 15 mL of acidified (2% HNO<sub>3</sub>, Optima grade) Milli-Q  
169 grade water. The amount of sample, spikes and dilution water were assessed by  
170 weighing. Reproducibility of this method is 1.5% (RSD) as tested on repeated  
171 preparations of reference solutions: SLRS-5 (NRC-CNRC river water reference  
172 material for trace metals; 101.9 ± 3.6 nmol kg<sup>-1</sup>) and a house-made reference of  
173 Mediterranean Sea water (deep water from the MOOSE DYFAMED site; 54.1  
174 nmol kg<sup>-1</sup>). The limit of detection, calculated as three times the standard deviation  
175 of the procedural blank, is 0.09 nmol kg<sup>-1</sup>.

176 Using the D\_Ba concentration, temperature, pressure and salinity data  
177 from the M84/3 cruise, we calculated the barite saturation index (SI) following the  
178 procedures described by Monnin et al. (1999) and Monnin and Cividini (2006). SI  
179 is defined as the Q/K ratio, where Q is the ionic product of aqueous barium  
180 sulphate, and K is the solubility product of barite. A saturation index value  
181 between 0.9 and 1.1 is taken to represent equilibrium (Monnin et al., 1999).  
182 Waters are considered to be undersaturated for SI <0.9.

183

### 184 3. RESULTS

185 Figure 3 shows the full-depth D\_Ba distribution for the Ionian and zonal  
186 sections, with the top 500 m expanded. The same scheme is reported for the barite  
187 saturation index (SI) in Figure 4. Figure 5 shows characteristic vertical D\_Ba  
188 profiles for the major sub-basins, as well as D\_Ba profiles for stations not  
189 included in the Ionian and zonal sections. Two broad features characterize the  
190 D\_Ba in the Mediterranean Sea: 1) a vertical gradient increasing from 38 nmol kg<sup>-1</sup>  
191 near the surface to 85 nmol kg<sup>-1</sup> at the bottom, with local deep D\_Ba maxima  
192 reaching up to 172 nmol kg<sup>-1</sup>, and 2) a pronounced water column undersaturation

193 with respect to barite ( $0.2 \leq SI \leq 0.6$ ) with a relative maximum in the intermediate  
194 waters at around 500 meters depth.

195 West of Gibraltar, in the Gulf of Cadiz, D\_Ba concentrations range from  
196 38 to 55 nmol kg<sup>-1</sup> in highly undersaturated waters (SI from 0.2 to 0.4) with only  
197 small vertical gradients (see representative D\_Ba profile at station #340 in Figure  
198 5a). The low D\_Ba and SI characteristic of AW can be followed throughout the  
199 surface waters of the Mediterranean Sea. For the upper 1000 m in the WMed, the  
200 D\_Ba distribution is marked by increasing D\_Ba concentration <70 nmol kg<sup>-1</sup>  
201 from west to east. In the EMed, the intermediate layer (200 to 700 m depth) is  
202 marked by slightly lower D\_Ba concentration (50 to 70 nmol kg<sup>-1</sup>) between 17  
203 and 26°E.

204 The deep (>1000 m) layers of the Mediterranean Sea are characterized by  
205 D\_Ba concentrations above 70 nmol kg<sup>-1</sup> with localized patches peaking up to 100  
206 nmol kg<sup>-1</sup>. Those are observed at 9.4°E in the WMed (station #321) and at 27.5°E  
207 in the EMed (station # 290) (see D\_Ba profiles in Figure 5f). Very high D\_Ba  
208 concentrations (139 and 172 nM, respectively) are furthermore found near the  
209 bottom at 33°E (station #291) and 21.5°E (station #301) (see D\_Ba profiles in  
210 Figure 5g). Note that very high D\_Ba contents (up to 160 nmol kg<sup>-1</sup>) are also  
211 found near the bottom at station #288 located at 26.2°E north-east of Crete (not  
212 shown in the zonal section; see D\_Ba profile in Figure 5g).

213 The same general features as reported for the zonal section are observed  
214 across the Ionian section, where the D\_Ba distribution is also marked by an  
215 increase in the water column D\_Ba content (from 48 to 95 nmol kg<sup>-1</sup>) in  
216 undersaturated waters (SI from 0.3 to 0.5). A SI maximum again extends in  
217 intermediate waters and lower D\_Ba concentrations (<70 nmol kg<sup>-1</sup>) occur

1  
2  
3  
4  
5  
6  
7  
8  
9  
10  
11  
12  
13  
14  
15  
16  
17  
18  
19  
20  
21  
22  
23  
24  
25  
26  
27  
28  
29  
30  
31  
32  
33  
34  
35  
36  
37  
38  
39  
40  
41  
42  
43  
44  
45  
46  
47  
48  
49  
50  
51  
52  
53  
54  
55  
56  
57  
58  
59  
60  
61  
62  
63  
64  
65

218 between 500 and 800 m along the Ionian section. The northern part of the Ionian  
219 section, north of the Otranto Strait (Adriatic Pit), is marked by relatively  
220 homogeneous D\_Ba concentrations ( $<65 \text{ nmol kg}^{-1}$ ) below 300 m (see D\_Ba  
221 profile at station #313 in Figure 5c). Also, a particular D\_Ba increase (up to 95  
222  $\text{nmol L}^{-1}$ ) is observed around a depth of 2000 m (station #307; see D\_Ba profile in  
223 Figure 5c). Note that a similar increase in D\_Ba concentrations around the same  
224 depth is detected at station #314 located in the area of station #307 (not shown in  
225 Fig.3; see D\_Ba profile in Figure 5c). D\_Ba increase around a depth of 2000 m is  
226 also observed in the EMed at stations #303 (southern Ionan Sea) and at stations  
227 #300 (24.3°E) and #298 (22.5°E) (not shown in Fig.3; see D\_Ba profiles in Figure  
228 5d).

229

#### 230 4. DISCUSSION

231 D\_Ba concentrations reported in the present work (from 38 to 100  $\text{nmol}$   
232  $\text{kg}^{-1}$ ) are of the same order of magnitude as D\_Ba values reported during previous  
233 Mediterranean cruises in the EMed (GEODYME data, Jeandel et al., pers. comm.)  
234 and in the WMed (Bernat et al., 1972; Dehairs et al., 1987; van Beek et al., 2009).  
235 Previous MedSea data are however relatively scarce, with in general limited  
236 vertical sampling resolution, preventing direct comparisons with the present data  
237 set. D\_Ba concentrations for the MedSea are also of the same order of magnitude  
238 as values reported for the Atlantic sector (Chan et al., 1977), the Indian and  
239 Southern Oceans (Jeandel et al., 1996; Jacquet et al., 2004, 2007, Hoppema et al.,  
240 2010) and for the North Pacific (Dehairs et al., 2008). Compared to the previous  
241 sectors, D\_Ba concentrations in the MedSea present however smaller vertical  
242 D\_Ba gradients which mainly range from 38 to 85  $\text{nmol kg}^{-1}$  between the surface

1  
2  
3  
4  
5  
6  
7  
8  
9  
10  
11  
12  
13  
14  
15  
16  
17  
18  
19  
20  
21  
22  
23  
24  
25  
26  
27  
28  
29  
30  
31  
32  
33  
34  
35  
36  
37  
38  
39  
40  
41  
42  
43  
44  
45  
46  
47  
48  
49  
50  
51  
52  
53  
54  
55  
56  
57  
58  
59  
60  
61  
62  
63  
64  
65

243 and the bottom. Our results indicate that the MedSea is undersaturated with  
244 respect to barite everywhere, in contrast to the above-mentioned oceans where  
245 saturation can be reached at certain locations (Monnin et al., 1999; Dehairs et al.,  
246 2008; Jacquet et al., 2008). SI exhibits a maximum value at depths around 500 m.  
247 Below these depths, the variations in D\_Ba concentration and temperature are  
248 small. The only factor affecting the SI value is pressure. The increase with  
249 pressure of the barite solubility product (K) is much larger than the increase of the  
250 aqueous barium sulphate ionic product (Q) which is proportional to the square of  
251 the activity coefficient of aqueous barium sulphate (Monnin et al., 1999; Monnin  
252 and Cividini, 2006). This results in a decrease of the barite SI with depth at depth  
253 ranges where D\_Ba and temperature are almost constant (i.e. the variations are too  
254 low to affect SI).

255 For the upper 1000 m, the general zonal D\_Ba pattern appears influenced  
256 by the water circulation in the Mediterranean basin. In the western part of the  
257 transect, the low D\_Ba contents and SI values coincide with the low-salinity  
258 surface AW flowing through the Strait of Gibraltar. The transition between AW  
259 and underlying LIW (referred to as MOW in the Gibraltar Strait) is marked by a  
260 steep vertical D\_Ba gradient (D\_Ba concentrations from <55 to >70 nmol kg<sup>-1</sup>). In  
261 the northern part of the Ionian section, the relatively homogeneous D\_Ba  
262 concentrations (at values <65 nmol kg<sup>-1</sup>) below 300 m result from the transition  
263 above the Otranto Strait from northward progressing LIW to less salty Adriatic  
264 waters potentially influenced by riverine input. Between 17 and 26°E in the  
265 EMed, low D\_Ba values (D\_Ba contents from 50 to 70 nmol kg<sup>-1</sup>) coincide in the  
266 upper 400 m with the sinking and westward progression of high density LIW  
267 (salinity maximum between 200 and 500 m). The sinking of isolines from east to

1  
2  
3  
4  
5  
6  
7  
8  
9  
10  
11  
12  
13  
14  
15  
16  
17  
18  
19  
20  
21  
22  
23  
24  
25  
26  
27  
28  
29  
30  
31  
32  
33  
34  
35  
36  
37  
38  
39  
40  
41  
42  
43  
44  
45  
46  
47  
48  
49  
50  
51  
52  
53  
54  
55  
56  
57  
58  
59  
60  
61  
62  
63  
64  
65

268 west in this zone is a feature also observed for other water mass properties  
269 (salinity, temperature, potential density and nutrients) (Tanhua et al., 2013b). It is  
270 furthermore possible that the extent of lower D\_Ba concentrations down to 700 m  
271 in this area reflects D\_Ba subtraction due to P\_Ba barite formation. The same is  
272 true for the lower D\_Ba concentrations reported along the Ionian section between  
273 500 and 800 m.

274         Concerning the deeper (>1000 m) water column, the high values of D\_Ba  
275 reported at 9.4°E and 27.5°E (up to 100 nmol kg<sup>-1</sup>) coincide with the top of  
276 seamounts. This Ba enrichment may be due to local dissolution of Ba-rich  
277 particles (barite) in the under-saturated water and would reflect epibenthic fluxes  
278 of Ba-rich particles that have been exported from the intermediate layers to the sea  
279 floor. This may also occur at station #291 (33°E) where the high D\_Ba value of  
280 139 nmol kg<sup>-1</sup> is found near the seafloor. The same is true for station #288 (north-  
281 east of Crete) where D\_Ba concentrations near the seafloor reach 160 nmol kg<sup>-1</sup>.  
282 Another source of very high D\_Ba concentrations in the MedSea could originate  
283 from the Black Sea where Moore and Falkner (1999) reported water column  
284 D\_Ba concentrations ranging from 130 to 500 nmol kg<sup>-1</sup>. No particularly high  
285 water column D\_Ba concentration is however reported at station #287 in the  
286 southern Eagean Sea, nor further south at station #289 located in the area of  
287 station #288 north-east of Crete (Fig.5e). A particular situation is also encountered  
288 at 21.5°E (station #301) where the highest D\_Ba concentration (172 nmol kg<sup>-1</sup>) of  
289 the whole dataset is found close to the “Atalante” brine lake, a water body with  
290 very high salinity (up to 160) and anoxic conditions. It has been well established  
291 that brines are highly concentrated in various elements (e.g. trace metals).  
292 Extremely high D\_Ba contents (up 670 nmol kg<sup>-1</sup>) resulting from sulphate salt

1  
2  
3  
4  
5  
6  
7  
8  
9  
10  
11  
12  
13  
14  
15  
16  
17  
18  
19  
20  
21  
22  
23  
24  
25  
26  
27  
28  
29  
30  
31  
32  
33  
34  
35  
36  
37  
38  
39  
40  
41  
42  
43  
44  
45  
46  
47  
48  
49  
50  
51  
52  
53  
54  
55  
56  
57  
58  
59  
60  
61  
62  
63  
64  
65

293 dissolution have for instance been reported in the Orca basin (Gulf of Mexico)  
294 (Schijf, 2007). The high D\_Ba contents reported at 21.5°E (station #301) in the  
295 EMed do not therefore reflect a higher export of Ba-rich particles to the seafloor,  
296 benthic processes, nor a possible influence of Black Sea waters, but rather an  
297 influence of the nearby brine lake.

298         The observed D\_Ba variation with depth (surface depletion and depth  
299 enrichment) is often referred to as a nutrient-like distribution. The precise  
300 mechanism shaping this D\_Ba distribution is still debated mainly because the  
301 control on barite formation inside POC micro-environments in undersaturated  
302 ocean waters is not fully resolved (Griffith and Paytan, 2012). The nutrient  
303 distribution during M84/3 (late winter-spring) is characterized by very low  
304 concentrations, in particular in the EMed (Tanhua et al., 2013b). The same trend  
305 was reported in previous studies emphasizing the increasing oligotrophic trend  
306 from west to east along the basin (Moutin and Raimbault, 2002; Pujo-Pay et al.,  
307 2011). The D\_Ba distribution is more uniform between WMed and EMed during  
308 M84/3 than reported for nutrients (Tanhua et al., 2013b). Also, the D\_Ba  
309 distribution is not fully depleted in surface waters and presents specific local  
310 depletions at intermediate depths. Jeandel et al. (1996) and Jacquet et al. (2007)  
311 reported a decoupling between D\_Ba and silicate and alkalinity distributions in  
312 the water column due to the fact that D\_Ba is not controlled by the same  
313 biogeochemical processes as those controlling the synthesis of opal and carbonate,  
314 and their dissolution. Throughout the whole basin, while barite is undersaturated,  
315 calcite and aragonite are largely supersaturated (Alvarez et al., 2014). This would  
316 explain decoupling between D\_Ba and total alkalinity in the deep waters (not  
317 shown; see Alvarez et al., 2014), as reflected by increasing D\_Ba concentrations

1  
2  
3  
4  
5  
6  
7  
8  
9  
10  
11  
12  
13  
14  
15  
16  
17  
18  
19  
20  
21  
22  
23  
24  
25  
26  
27  
28  
29  
30  
31  
32  
33  
34  
35  
36  
37  
38  
39  
40  
41  
42  
43  
44  
45  
46  
47  
48  
49  
50  
51  
52  
53  
54  
55  
56  
57  
58  
59  
60  
61  
62  
63  
64  
65

318 despite constant total alkalinity in the water column below 1000 m, especially in  
319 the EMed. The D\_Ba enrichment in deep waters reflects dissolution of Ba-rich  
320 particles produced at intermediate depths and exported to the sea floor. This D\_Ba  
321 increase may be enhanced by the residence time and ventilation of deep waters.  
322 Studies of transient tracers (CFC-12, SF<sub>6</sub> and tritium) over the last two decades  
323 revealed a period of low ventilation in the deep eastern (Levantine) basin, while  
324 the WMed was marked by massive input of recently ventilated water (Ströven and  
325 Tanhua, 2013; Schneider et al., 2014; Schröder et al., 2008, 2010). These  
326 differences in the ventilation of deep water masses could explain the fact that the  
327 extent of high D\_Ba values is larger in the EMed than in the WMed. Nevertheless,  
328 the fact that over the basin the D\_Ba concentration increases with depth indicates  
329 dissolution of Ba-rich particles produced at intermediate depths during POC  
330 remineralization processes and transferred through the deep water. Our results  
331 indicate that this transfer of Ba-rich particles is more important at 9°E in the  
332 WMed and east of 25°E in the EMed (i.e. D\_Ba contents >80 nmol kg<sup>-1</sup>). The  
333 particulate and dissolved organic carbon (POC, DOC) dynamics in the MedSea  
334 are relatively complex (Lefèvre et al., 1996; Santinelli et al., 2010; Lopez-  
335 Sandoval et al., 2011; Luna et al., 2012). It is therefore difficult to discuss in detail  
336 the link between the deep water column transfer of Ba-enriched particles and  
337 sinking POC.

338

## 339 **5. CONCLUSION**

340 The present paper presents an extended data set on the D\_Ba distribution  
341 along a high resolution and quasi-zonal transect in the MedSea in late winter-  
342 spring 2011. Our results reveal that the D\_Ba distribution appears driven by

1  
2  
3  
4  
5  
6  
7  
8  
9  
10  
11  
12  
13  
14  
15  
16  
17  
18  
19  
20  
21  
22  
23  
24  
25  
26  
27  
28  
29  
30  
31  
32  
33  
34  
35  
36  
37  
38  
39  
40  
41  
42  
43  
44  
45  
46  
47  
48  
49  
50  
51  
52  
53  
54  
55  
56  
57  
58  
59  
60  
61  
62  
63  
64  
65

343 hydrodynamics, while enhanced D\_Ba contents in deep waters could reflect the  
344 effect of a higher P\_Ba barite flux in undersaturated water. Also, the occurrence  
345 of lower D\_Ba contents at intermediate depths could reflect horizons of intense  
346 particulate and dissolved Ba dynamics. In order to further constrain the link  
347 between these specific features of the D\_Ba distribution and the organic carbon  
348 dynamics in the MedSea, the sensitivity of the Ba signal to the phytoplankton  
349 growth season and to dense-water formation events should be addressed.

350

### 351 **Acknowledgements**

352 For their support to this research, we thank the captain and crew of R/V  
353 *Meteor*. R. Brünjes (GEOMAR) took the barium samples during the M84/3  
354 cruise. S. Chifflet (MIO) helped for samples processing. This research was  
355 supported by French LEFE CYBER grant (BADIMED project; 2014-2015). The  
356 HR-ICP-MS (ELEMENT XR, Thermo) was supported in 2012 by European  
357 Regional Development Fund (ERDF). The M84/3 cruise was supported by a grant  
358 from the Deutsche Forschungsgemeinschaft (DFG)- Senatskommission für  
359 Ozeanographie, and from a grant from DFG [TA 317/3-1]. Authors thank the  
360 Labex OT- Med (ANR-11-LABEX-0061) funded by the « Investissements  
361 d'Avenir », French Government project of the French National Research Agency  
362 (ANR) through the A\*Midex project (ANR-11-IDEX-0001-02), for enhancing  
363 networking of the BADIMED project. LJ acknowledges the support of the  
364 European Union via a Marie Curie fellowship (FP7-PEOPLE-2012-IEF no  
365 328416).

366

### 367 **Figure captions**



368

369 Figure 1: Map of the Mediterranean Sea with the stations (blue dots) of the M84/3  
370 cruise where samples were taken for the analysis of dissolved barium, along with  
371 the bathymetry of the basins. WMED: Western Mediterranean Sea, EMED:  
372 Eastern Mediterranean Sea. Figure constructed using Ocean Data View (Schlitzer,  
373 2003).

374

375 Figure 2: Potential temperature – salinity diagram with isopycnals ( $\text{kg m}^{-3}$ ) of the  
376 whole data set (a) and focus on deep waters (b). Colors represent the  
377 concentration of D\_Ba in  $\text{nmol kg}^{-1}$ . WMed, EMed: Western and Eastern  
378 Mediterranean Sea. AW= Atlantic Water, MOW= Mediterranean Overflow  
379 Water, ISW= Ionian Surface Water, LSW= Levantine Surface Water, LIW=  
380 Levantine Intermediate Water, CIW= Cretan Intermediate Water, WMDW=  
381 Western Mediterranean Deep Water, AddW= Adriatic Deep Water, CDW=  
382 Cretan Deep Water.

383

384 Figure 3: Sections of D\_Ba distribution ( $\text{nmol kg}^{-1}$ ) in the Mediterranean Sea from  
385 the Meteor cruise M84/3 (April 2011). The top-right panel is a meridional section  
386 from the Adriatic Sea to the Ionian sea (light grey line on the map) and the lower  
387 panel is the zonal section from the coast of Lebanon in the EMed to the Strait of  
388 Gibraltar in the WMed (dark grey line on the map). The depth scale and the color  
389 scale are identical for all panels. The top 500 m in each section and associated  
390 color scale are slightly expanded.

391

392 Figure 4: Similar to Fig.3, but for barite saturation index (SI).

393

394 Figure 5: Characteristic vertical D\_Ba profiles for the major sub-basins and D\_Ba  
395 profiles for stations not included in the Ionian and zonal sections.

396

397 **References**

398 Álvarez, M., Sanleón-Bartolomé, H., Tanhua, T., Mintrop, L., Luchetta, A.,  
399 Cantoni, C., Schroeder, K., Civitarese, G., 2014. The CO<sub>2</sub> system in the  
400 Mediterranean Sea: a basin wide perspective. *Ocean Sci.* 10, 69–92.  
401 doi:10.5194/os-10-69-2014

402 Bernat, M., Church, T., Allegre, C.J., 1972. Barium and strontium concentrations  
403 in Pacific and Mediterranean sea water profiles by direct isotope dilution  
404 mass spectrometry. *Earth and Planetary Science Letters* 16, 75–80.  
405 doi:10.1016/0012-821X(72)90238-5

406 Cardinal, D., Savoye, N., Trull, T.W., André, L., Kopczynska, E.E., Dehairs, F.,  
407 2005. Variations of carbon remineralisation in the Southern Ocean illustrated  
408 by the Baxs proxy. *Deep Sea Research Part I: Oceanographic Research*  
409 *Papers* 52, 355–370. doi:10.1016/j.dsr.2004.10.002

410 Chan, L.H., Drummond, D., Edmond, J.M., Grant, B., 1977. On the barium data  
411 from the Atlantic GEOSECS expedition. *Deep Sea Research* 24, 613–649.  
412 doi:10.1016/0146-6291(77)90505-7

413 Dehairs, F., Chesselet, R., Jedwab, J., 1980. Discrete suspended particles of barite  
414 and the barium cycle in the open ocean. *Earth and Planetary Science Letters*  
415 49, 528–550. doi:10.1016/0012-821X(80)90094-1

416 Dehairs, F., Jacquet, S., Savoye, N., Van Mooy, B.A.S., Buesseler, K.O., Bishop,  
417 J.K.B., Lamborg, C.H., Elskens, M., Baeyens, W., Boyd, P.W., Casciotti,

1  
2  
3  
4  
5  
6  
7  
8  
9  
10  
11  
12  
13  
14  
15  
16  
17  
18  
19  
20  
21  
22  
23  
24  
25  
26  
27  
28  
29  
30  
31  
32  
33  
34  
35  
36  
37  
38  
39  
40  
41  
42  
43  
44  
45  
46  
47  
48  
49  
50  
51  
52  
53  
54  
55  
56  
57  
58  
59  
60  
61  
62  
63  
64  
65

418 K.L., Monnin, C., 2008. Barium in twilight zone suspended matter as a  
419 potential proxy for particulate organic carbon remineralization: Results for  
420 the North Pacific. *Deep Sea Research Part II: Topical Studies in*  
421 *Oceanography, Understanding the Ocean's Biological Pump: results from*  
422 *VERTIGO* 55, 1673–1683. doi:10.1016/j.dsr2.2008.04.020

423 Dehairs, F., Lambert, C.E., Chesselet, R., Risler, N., 1987. The biological  
424 production of marine suspended barite and the barium cycle in the Western  
425 Mediterranean Sea. *Biogeochemistry* 4, 119–140. doi:10.1007/BF02180151

426 Dehairs, F., Shopova, D., Ober, S., Veth, C., Goeyens, L., 1997. Particulate  
427 barium stocks and oxygen consumption in the Southern Ocean mesopelagic  
428 water column during spring and early summer: relationship with export  
429 production. *Deep Sea Research Part II: Topical Studies in Oceanography* 44,  
430 497–516. doi:10.1016/S0967-0645(96)00072-0

431 Durrieu de Madron, X., Guieu, C., Sempéré, R., Conan, P., Cossa, D., D'Ortenzio,  
432 F., Estournel, C., Gazeau, F., Rabouille, C., Stemmann, L., Bonnet, S., Diaz,  
433 F., Koubbi, P., Radakovitch, O., Babin, M., Baklouti, M., Bancon-Montigny,  
434 C., Belviso, S., Bensoussan, N., Bonsang, B., Bouloubassi, I., Brunet, C.,  
435 Cadiou, J.-F., Carlotti, F., Chami, M., Charmasson, S., Charrière, B., Dachs,  
436 J., Doxaran, D., Dutay, J.-C., Elbaz-Poulichet, F., Eléaume, M., Eyrolles, F.,  
437 Fernandez, C., Fowler, S., Francour, P., Gaertner, J.C., Galzin, R., Gasparini,  
438 S., Ghiglione, J.-F., Gonzalez, J.-L., Goyet, C., Guidi, L., Guizien, K.,  
439 Heimbürger, L.-E., Jacquet, S.H.M., Jeffrey, W.H., Joux, F., Le Hir, P.,  
440 Leblanc, K., Lefèvre, D., Lejeusne, C., Lemé, R., Loye-Pilot, M.-D., Mallet,  
441 M., Méjanelle, L., Mélin, F., Mellon, C., Méricot, B., Merle, P.-L., Migon,  
442 C., Miller, W.L., Mortier, L., Mostajir, B., Mousseau, L., Moutin, T., Para,

1  
2  
3  
4  
5  
6  
7  
8  
9  
10  
11  
12  
13  
14  
15  
16  
17  
18  
19  
20  
21  
22  
23  
24  
25  
26  
27  
28  
29  
30  
31  
32  
33  
34  
35  
36  
37  
38  
39  
40  
41  
42  
43  
44  
45  
46  
47  
48  
49  
50  
51  
52  
53  
54  
55  
56  
57  
58  
59  
60  
61  
62  
63  
64  
65

443 J., Pérez, T., Petrenko, A., Poggiale, J.-C., Prieur, L., Pujó-Pay, M., Pulido-  
444 Villena, Raimbault, P., Rees, A.P., Ridame, C., Rontani, J.-F., Ruiz Pino, D.,  
445 Sicre, M.A., Taillandier, V., Tamburini, C., Tanaka, T., Taupier-Letage, I.,  
446 Tedetti, M., Testor, P., Thébault, H., Thouvenin, B., Touratier, F.,  
447 Tronczynski, J., Ulses, C., Van Wambeke, F., Vantrepotte, V., Vaz, S.,  
448 Verney, R., 2011. Marine ecosystems' responses to climatic and  
449 anthropogenic forcings in the Mediterranean. *Progress in Oceanography* 91,  
450 97–166. doi:10.1016/j.pocean.2011.02.003

451 Freydier, R., Dupre, B., Polve, M., 1995. Analyses by Inductively-Coupled  
452 Plasma-Mass Spectrometry of Ba Concentrations in Water and Rock  
453 Samples - Comparison Between Isotope-Dilution and External Calibration  
454 with or Without Internal Standard. *Eur. Mass Spectrom.* 1, 283–291.  
455 doi:10.1255/ejms.140

456 Griffith, E.M., Paytan, A., 2012. Barite in the ocean – occurrence, geochemistry  
457 and palaeoceanographic applications. *Sedimentology* 59, 1817–1835.  
458 doi:10.1111/j.1365-3091.2012.01327

459 Durrieu de Madron, X., Houpert, L., Puig, P., Sanchez-Vidal, A., Testor, P.,  
460 Bosse, A., Estournel, C., Somot, S., Bourrin, F., Bouin, M.N., Beauverger,  
461 M., Beguery, L., Calafat, A., Canals, M., Cassou, C., Coppola, L., Dausse,  
462 D., D'Ortenzio, F., Font, J., Heussner, S., Kunesch, S., Lefevre, D., Le Goff,  
463 H., Martín, J., Mortier, L., Palanques, A., Raimbault, P., 2013. Interaction of  
464 dense shelf water cascading and open-sea convection in the northwestern  
465 Mediterranean during winter 2012. *Geophys. Res. Lett.* 40, 1379–1385.  
466 doi:10.1002/grl.50331

1  
2  
3  
4  
5  
6  
7  
8  
9  
10  
11  
12  
13  
14  
15  
16  
17  
18  
19  
20  
21  
22  
23  
24  
25  
26  
27  
28  
29  
30  
31  
32  
33  
34  
35  
36  
37  
38  
39  
40  
41  
42  
43  
44  
45  
46  
47  
48  
49  
50  
51  
52  
53  
54  
55  
56  
57  
58  
59  
60  
61  
62  
63  
64  
65

467 Hainbucher, D., Rubino, A., Cardin, V., Tanhua, T., Schroeder, K., Bensi, M.,  
468 2014. Hydrographic situation during cruise M84/3 and P414 (spring 2011) in  
469 the Mediterranean Sea. *Ocean Sci.* 10, 669–682. doi:10.5194/os-10-669-2014  
470 Hoppema, M., Dehairs, F., Navez, J., Monnin, C., Jeandel, C., Fahrbach, E., de  
471 Baar, H.J.W., 2010. Distribution of barium in the Weddell Gyre: Impact of  
472 circulation and biogeochemical processes. *Marine Chemistry* 122, 118–129.  
473 doi:10.1016/j.marchem.2010.07.005  
474 Jacquet, S.H.M., Dehairs, F., Cardinal, D., Navez, J., Delille, B., 2005. Barium  
475 distribution across the Southern Ocean frontal system in the Crozet–  
476 Kerguelen Basin. *Marine Chemistry* 95, 149–162.  
477 doi:10.1016/j.marchem.2004.09.002  
478 Jacquet, S.H.M., Dehairs, F., Dumont, I., Becquevort, S., Cavagna, A.-J.,  
479 Cardinal, D., 2011. Twilight zone organic carbon remineralization in the  
480 Polar Front Zone and Subantarctic Zone south of Tasmania. *Deep Sea*  
481 *Research Part II: Topical Studies in Oceanography, Biogeochemistry of the*  
482 *Australian Sector of the Southern Ocean* 58, 2222–2234.  
483 doi:10.1016/j.dsr2.2011.05.029  
484 Jacquet, S.H.M., Dehairs, F., Elskens, M., Savoye, N., Cardinal, D., 2007. Barium  
485 cycling along WOCE SR3 line in the Southern Ocean. *Marine Chemistry*,  
486 *Special issue: Dedicated to the memory of Professor Roland Wollast* 106,  
487 33–45. doi:10.1016/j.marchem.2006.06.007  
488 Jacquet, S.H.M., Dehairs, F., Lefèvre, D., Cavagna, A.J., Planchon, F., Christaki,  
489 U., Monin, L., André, L., Closset, I., Cardinal, D., 2015. Early spring  
490 mesopelagic carbon remineralization and transfer efficiency in the naturally

1  
2  
3  
4  
5  
6  
7  
8  
9  
10  
11  
12  
13  
14  
15  
16  
17  
18  
19  
20  
21  
22  
23  
24  
25  
26  
27  
28  
29  
30  
31  
32  
33  
34  
35  
36  
37  
38  
39  
40  
41  
42  
43  
44  
45  
46  
47  
48  
49  
50  
51  
52  
53  
54  
55  
56  
57  
58  
59  
60  
61  
62  
63  
64  
65

491 iron-fertilized Kerguelen area. *Biogeosciences* 12, 1713–1731.  
492 doi:10.5194/bg-12-1713-2015

493 Jacquet, S.H.M., Dehairs, F., Rintoul, S., 2004. A high resolution transect of  
494 dissolved barium in the Southern Ocean. *Geophys. Res. Lett.* 31, L14301.  
495 doi:10.1029/2004GL020016

496 Jacquet, S.H.M., Dehairs, F., Savoye, N., Obernosterer, I., Christaki, U., Monnin,  
497 C., Cardinal, D., 2008. Mesopelagic organic carbon remineralization in the  
498 Kerguelen Plateau region tracked by biogenic particulate Ba. *Deep Sea*  
499 *Research Part II: Topical Studies in Oceanography, KEOPS: Kerguelen*  
500 *Ocean and Plateau compared Study* 55, 868–879.  
501 doi:10.1016/j.dsr2.2007.12.038

502 Jeandel, C., Dupré, B., Lebaron, G., Monnin, C., Minster, J.-F., 1996.  
503 Longitudinal distributions of dissolved barium, silica and alkalinity in the  
504 western and southern Indian Ocean. *Deep Sea Research Part I: Oceanographic Research Papers* 43, 1–31. doi:10.1016/0967-0637(95)00098-  
505 4  
506

507 Klinkhammer, G.P., Chan, L.H., 1990. Determination of barium in marine waters  
508 by isotope dilution inductively coupled plasma mass spectrometry. *Analytica*  
509 *Chimica Acta* 232, 323–329. doi:10.1016/S0003-2670(00)81249-0

510 Lefèvre, D., Denis, M., Lambert, C.E., Miquel, J.-C., 1996. Is DOC the main  
511 source of organic matter remineralization in the ocean water column? *Journal*  
512 *of Marine Systems, The Coastal Ocean in a Global Change Perspective* 7,  
513 281–291. doi:10.1016/0924-7963(95)00003-8

1  
2  
3  
4  
5  
6  
7  
8  
9  
10  
11  
12  
13  
14  
15  
16  
17  
18  
19  
20  
21  
22  
23  
24  
25  
26  
27  
28  
29  
30  
31  
32  
33  
34  
35  
36  
37  
38  
39  
40  
41  
42  
43  
44  
45  
46  
47  
48  
49  
50  
51  
52  
53  
54  
55  
56  
57  
58  
59  
60  
61  
62  
63  
64  
65

514 López-Sandoval, D.C., Fernández, A., Marañón, E., 2011. Dissolved and  
515 particulate primary production along a longitudinal gradient in the  
516 Mediterranean Sea. *Biogeosciences* 8, 815–825. doi:10.5194/bg-8-815-2011  
517 Luna, G.M., Bianchelli, S., Decembrini, F., De Domenico, E., Danovaro, R.,  
518 Dell’Anno, A., 2012. The dark portion of the Mediterranean Sea is a  
519 bioreactor of organic matter cycling. *Global Biogeochem. Cycles* 26,  
520 GB2017. doi:10.1029/2011GB004168  
521 Malanotte-Rizzoli, P., Artale, V., Borzelli-Eusebi, G.L., Brenner, S., Crise, A.,  
522 Gacic, M., Kress, N., Marullo, S., Ribera d’Alcalà, M., Sofianos, S., Tanhua,  
523 T., Theocharis, A., Alvarez, M., Ashkenazy, Y., Bergamasco, A., Cardin, V.,  
524 Carniel, S., Civitarese, G., D’Ortenzio, F., Font, J., Garcia-Ladona, E.,  
525 Garcia-Lafuente, J.M., Gogou, A., Gregoire, M., Hainbucher, D.,  
526 Kontoyannis, H., Kovacevic, V., Kraskapoulou, E., Kroskos, G., Incarbona,  
527 A., Mazzocchi, M.G., Orlic, M., Ozsoy, E., Pascual, A., Poulain, P.-M.,  
528 Roether, W., Rubino, A., Schroeder, K., Siokou-Frangou, J.,  
529 Souvermezoglou, E., Sprovieri, M., Tintoré, J., Triantafyllou, G., 2014.  
530 Physical forcing and physical/biochemical variability of the Mediterranean  
531 Sea: a review of unresolved issues and directions for future research. *Ocean*  
532 *Science* 10, 281–322. doi:10.5194/os-10-281-2014  
533 Monnin, C., Cividini, D., 2006. The saturation state of the world’s ocean with  
534 respect to (Ba,Sr)SO<sub>4</sub> solid solutions. *Geochimica et Cosmochimica Acta* 70,  
535 3290–3298. doi:10.1016/j.gca.2006.04.002  
536 Monnin, C., Jeandel, C., Cattaldo, T., Dehairs, F., 1999. The marine barite  
537 saturation state of the world’s oceans. *Marine Chemistry* 65, 253–261.  
538 doi:10.1016/S0304-4203(99)00016-X

- 1  
2  
3  
4  
5  
6  
7  
8  
9  
10  
11  
12  
13  
14  
15  
16  
17  
18  
19  
20  
21  
22  
23  
24  
25  
26  
27  
28  
29  
30  
31  
32  
33  
34  
35  
36  
37  
38  
39  
40  
41  
42  
43  
44  
45  
46  
47  
48  
49  
50  
51  
52  
53  
54  
55  
56  
57  
58  
59  
60  
61  
62  
63  
64  
65
- 539 Moore, W.S., Falkner, K.K., 1999. Cycling of radium and barium in the Black  
540 Sea. *Journal of Environmental Radioactivity* 43, 247–254.  
541 doi:10.1016/S0265-931X(98)00095-2
- 542 Ostlund, H.G., et al, 1987. GEOSECS Atlantic, Pacific, and Indian Ocean  
543 Expeditions Vol 7 [WWW Document]. EPIC3 Washington, D.C., NSF. URL  
544 <http://epic.awi.de/34890/> (accessed 4.13.15).
- 545 Reygondeau, G, Irisson J-O, Guieu C, Gasparini S, Ayata, S-D, P. Koubbi, 2013.  
546 Toward a dynamic biogeochemical division of the Mediterranean Sea in a  
547 context of global climate change. EGU General Assembly 2013, Vienna,  
548 Austria, 07–12 April 2013. Available at:  
549 <http://meetingorganizer.copernicus.org/EGU2013/EGU2013-10011.pdf>.
- 550 Roether, W., Manca, B.B., Klein, B., Bregant, D., Georgopoulos, D., Beitzel, V.,  
551 Kovačević, V., Luchetta, A., 1996. Recent Changes in Eastern Mediterranean  
552 Deep Waters. *Science* 271, 333–335. doi:10.1126/science.271.5247.333
- 553 Rushdi, A.I., McManus, J., Collier, R.W., 2000. Marine barite and celestite  
554 saturation in seawater. *Marine Chemistry* 69, 19–31. doi:10.1016/S0304-  
555 4203(99)00089-4
- 556 Santinelli, C., Nannicini, L., Seritti, A., 2010. DOC dynamics in the meso and  
557 bathypelagic layers of the Mediterranean Sea. *Deep Sea Research Part II:*  
558 *Topical Studies in Oceanography, Ecological and Biogeochemical*  
559 *Interactions in the Dark Ocean* 57, 1446–1459.  
560 doi:10.1016/j.dsr2.2010.02.014
- 561 Schijf, J., 2007. Alkali elements (Na, K, Rb) and alkaline earth elements (Mg, Ca,  
562 Sr, Ba) in the anoxic brine of Orca Basin, northern Gulf of Mexico. *Chemical*  
563 *Geology* 243, 255–274. doi:10.1016/j.chemgeo.2007.06.011



1  
2  
3  
4  
5  
6  
7  
8  
9  
10  
11  
12  
13  
14  
15  
16  
17  
18  
19  
20  
21  
22  
23  
24  
25  
26  
27  
28  
29  
30  
31  
32  
33  
34  
35  
36  
37  
38  
39  
40  
41  
42  
43  
44  
45  
46  
47  
48  
49  
50  
51  
52  
53  
54  
55  
56  
57  
58  
59  
60  
61  
62  
63  
64  
65

564 Schlitzer, R., 2003. Ocean Data View, [http://www.awi-](http://www.awi-bremerhaven.de/GEO/ODV)  
565 [bremerhaven.de/GEO/ODV](http://www.awi-bremerhaven.de/GEO/ODV)  
566 Schneider, A., Tanhua, T., Roether, W., Steinfeldt, R., 2014. Changes in  
567 ventilation of the Mediterranean Sea during the past 25 year. *Ocean Sci.* 10,  
568 1–16. doi:10.5194/os-10-1-2014  
569 Schott, F., Visbeck, M., Send, U., Fischer, J., Stramma, L., Desaubies, Y., 1996.  
570 Observations of Deep Convection in the Gulf of Lions, Northern  
571 Mediterranean, during the Winter of 1991/92. *Journal of Physical*  
572 *Oceanography* 26, 505–524. doi:10.1175/1520-  
573 0485(1996)026<0505:OODCIT>2.0.CO;2  
574 Schroeder, K., Josey, S.A., Herrmann, M., Grignon, L., Gasparini, G.P., Bryden,  
575 H.L., 2010. Abrupt warming and salting of the Western Mediterranean Deep  
576 Water after 2005: Atmospheric forcings and lateral advection. *J. Geophys.*  
577 *Res.* 115, C08029. doi:10.1029/2009JC005749  
578 Schroeder, K., Ribotti, A., Borghini, M., Sorgente, R., Perilli, A., Gasparini, G.P.,  
579 2008. An extensive western Mediterranean deep water renewal between 2004  
580 and 2006. *Geophys. Res. Lett.* 35, L18605. doi:10.1029/2008GL035146  
581 Shopova, D., Dehairs, F., Baeyens, W., 1995. A simple model of biogeochemical  
582 element distribution in the oceanic water column. *Journal of Marine Systems*  
583 6, 331–344. doi:10.1016/0924-7963(94)00032-7  
584 Stöven, T., Tanhua, T., 2014. Ventilation of the Mediterranean Sea constrained by  
585 multiple transient tracer measurements. *Ocean Sci.* 10, 439–457.  
586 doi:10.5194/os-10-439-2014  
587 Tanhua, T., Hainbucher, D., Cardin, V., Álvarez, M., Civitarese, G., McNichol,  
588 A.P., Key, R.M., 2013a. Repeat hydrography in the Mediterranean Sea, data

1  
2  
3  
4  
5  
6  
7  
8  
9  
10  
11  
12  
13  
14  
15  
16  
17  
18  
19  
20  
21  
22  
23  
24  
25  
26  
27  
28  
29  
30  
31  
32  
33  
34  
35  
36  
37  
38  
39  
40  
41  
42  
43  
44  
45  
46  
47  
48  
49  
50  
51  
52  
53  
54  
55  
56  
57  
58  
59  
60  
61  
62  
63  
64  
65

589 from the *Meteor* cruise 84/3 in 2011. *Earth System*  
590 *Science Data* 5, 289–294. doi:10.5194/essd-5-289-2013  
591 Tanhua, T., Hainbucher, D., Schroeder, K., Cardin, V., Álvarez, M., Civitarese,  
592 G., 2013b. The Mediterranean Sea system: a review and an introduction to  
593 the special issue. *Ocean Sci.* 9, 789–803. doi:10.5194/os-9-789-2013  
594 Van Beek, P., Sternberg, E., Reyss, J.-L., Souhaut, M., Robin, E., Jeandel, C.,  
595 2009.  $^{228}\text{Ra}/^{226}\text{Ra}$  and  $^{226}\text{Ra}/\text{Ba}$  ratios in the Western Mediterranean Sea:  
596 Barite formation and transport in the water column. *Geochimica et*  
597 *Cosmochimica Acta* 73, 4720–4737. doi:10.1016/j.gca.2009.05.063

Figure2

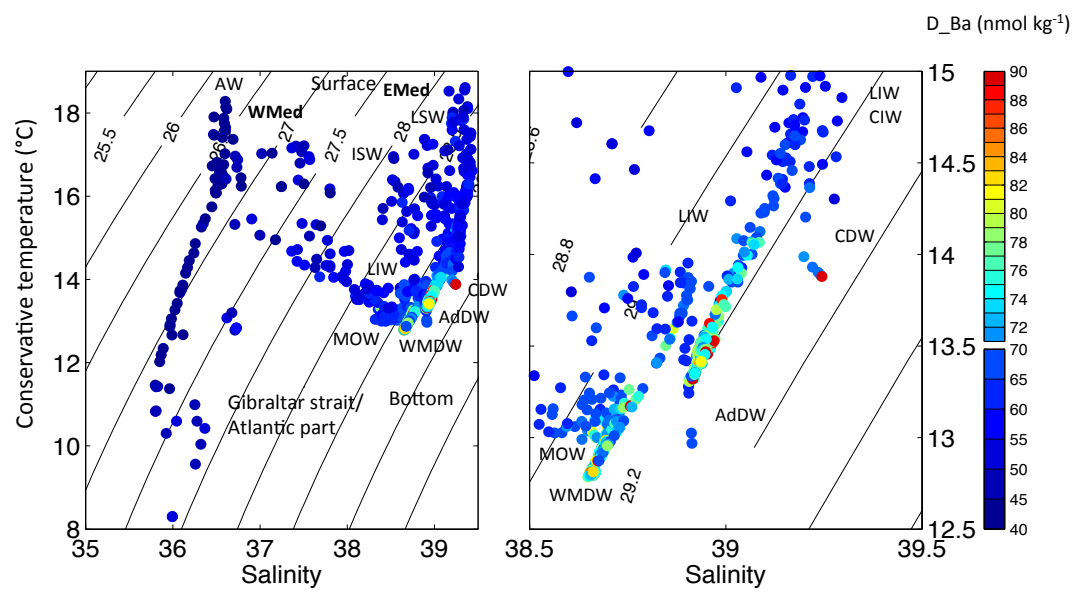


Figure3

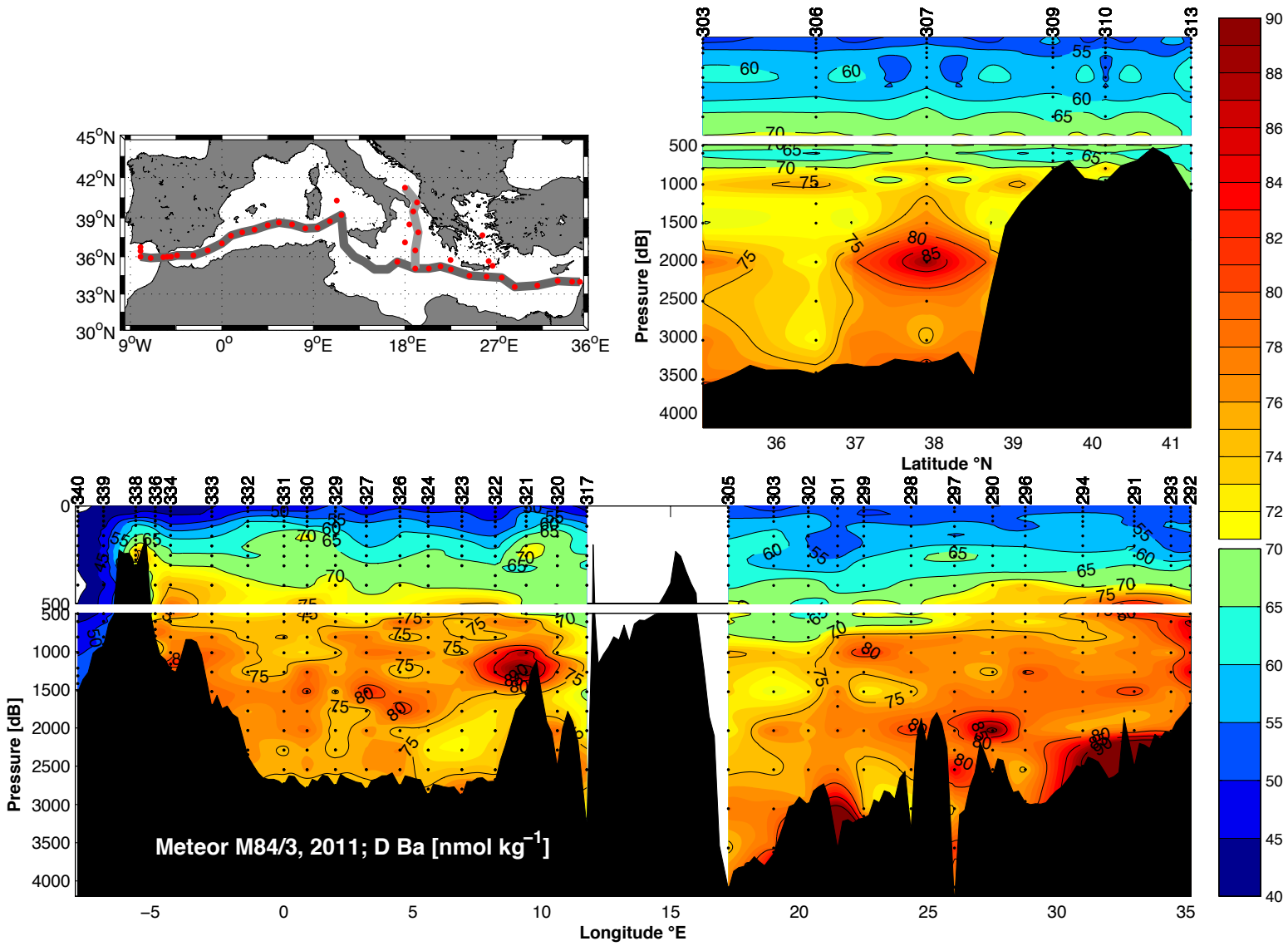


Figure4

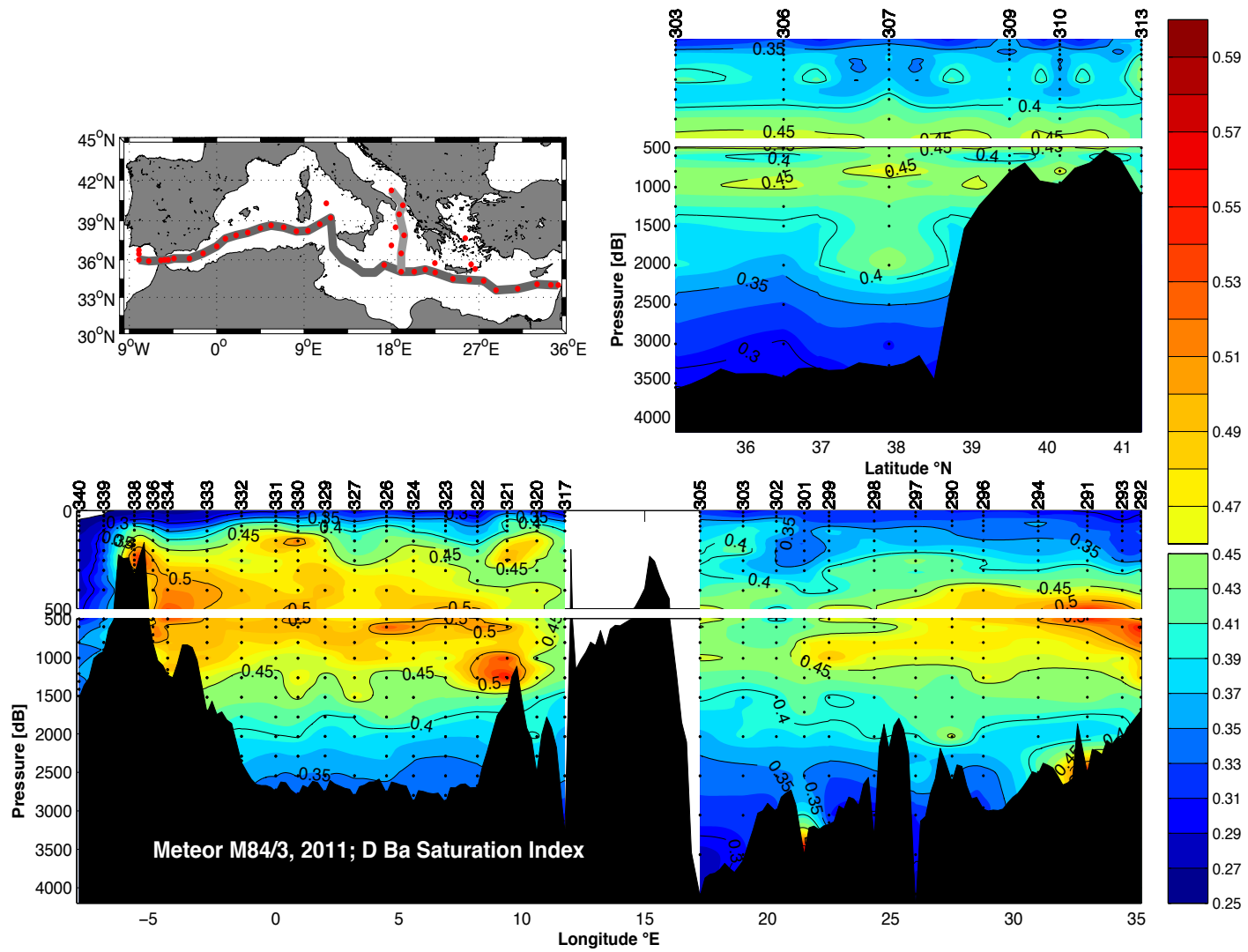
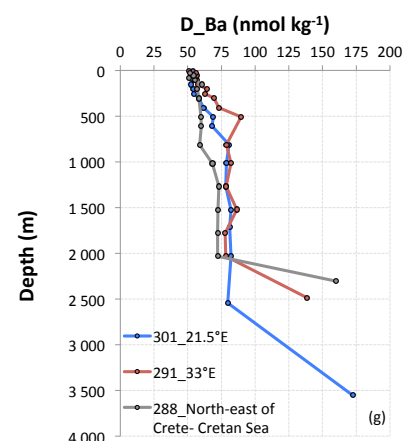
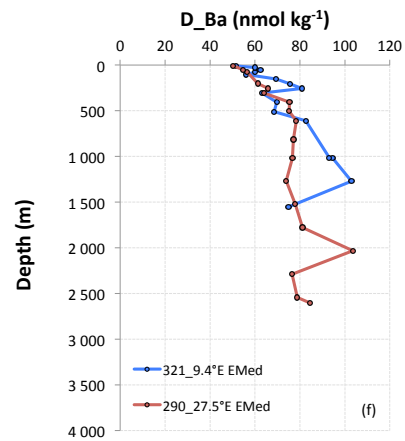
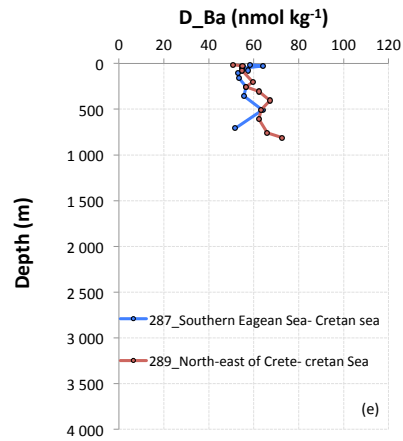
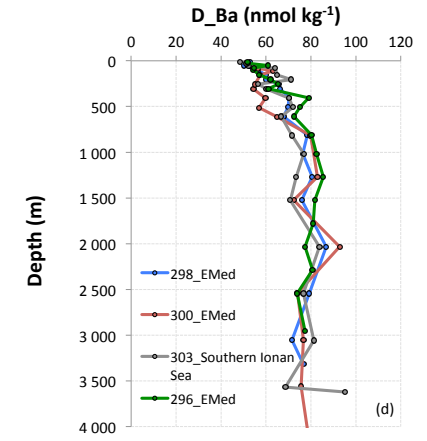
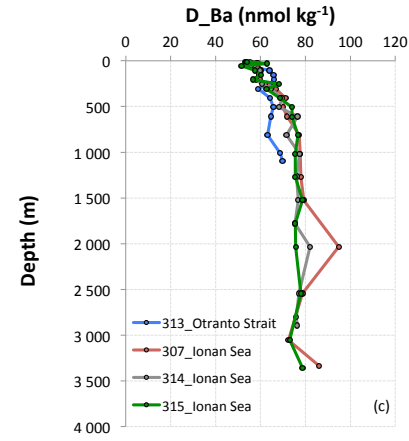
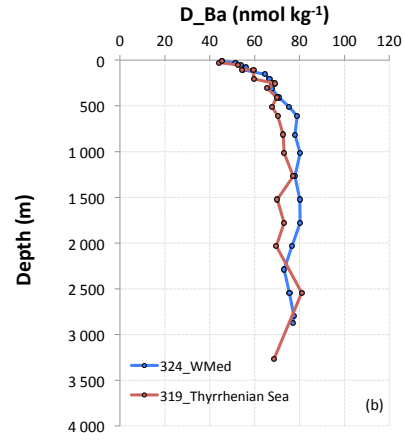
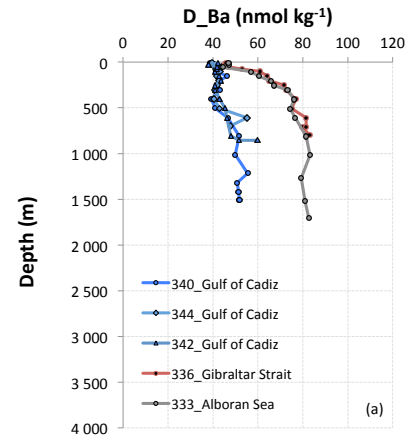


Figure5



D<sub>Ba</sub> is investigated along a high resolution and quasi-zonal transect in the MedSea.

The D<sub>Ba</sub> content ranges from 38 to 85 nmol kg<sup>-1</sup> with local deep D<sub>Ba</sub> maxima reaching up to 172 nmol kg<sup>-1</sup>

The water column is largely undersaturated with respect to barite ( $0.2 < SI < 0.6$ ).

The D<sub>Ba</sub> distribution is impacted by the large-scale Mediterranean circulation and biogeochemical processes.

Local changes in the D<sub>Ba</sub> patterns may be key to better constrain the C dynamics in the MedSea.